The effect of increasing surface cover vegetation on urban microclimate and energy demand for building heating and cooling

Evyatar Erell, Bin Zhou

Angaben zur Veröffentlichung / Publication details:

Erell, Evyatar, and Bin Zhou. 2022. "The effect of increasing surface cover vegetation on urban microclimate and energy demand for building heating and cooling." *Building and Environment* 213: 108867. https://doi.org/10.1016/j.buildenv.2022.108867.

The effect of increasing surface cover vegetation on urban microclimate and energy demand for building heating and cooling

Evyatar Erell *, Bin Zhou

Ben-Gurion University of the Negev, Israel

ARTICLE INFO

Keywords:
Building energy simulation
Climate cooling potential
Computer modelling
Vegetation
Mitigation
Urban heat islands

ABSTRACT

The study examines the potential effects of adding vegetation to an urban neighborhood in Tel Aviv on the microclimate, and subsequently on the potential for cooling by night ventilation and on energy consumption for heating and air conditioning. Computer simulation was employed to first generate modified weather files that account for urban effects of location, surface cover and density in different building configurations. These files were then used to assess the climatic cooling potential (CCP) by night ventilation and as inputs for detailed computer simulation of building energy performance. The microclimate model simulation indicates that elevated urban night-time temperatures will increase summer cooling loads relative to the reference rural site, but this penalty will be more than offset by reduced winter heating loads, resulting in a net decrease of between 2 and 7% in electricity use for heating and cooling (depending on building characteristics). The main impact of the urban heat island in this case is the reduction in the potential for cooling by night ventilation, which is almost completely absent in the summer months. Consequently, the urban climate of Tel Aviv may increase the prevalence of air conditioning use and will make buildings more vulnerable to potential loss of electric power in case of shortages or blackouts during episodes of extreme heat. Implementing a strategy of extensive planting, so that a green surface fraction of 0.5 is obtained, results in a mean annual temperature reduction of about 0.3 °C and an energy saving relative to the current condition of about 2–3%.

1. Introduction

The contribution of vegetation to urban heat island (UHI) mitigation is supported by numerous studies: employing remote sensing techniques, in particular satellite thermal imaging [1–5]; field studies comparing 'green' neighborhoods to 'grey' ones [6–8]; and computer simulation [9–13]. The implicit assumption, often stated explicitly, is that 'heat island mitigation' will necessarily lead to savings in building energy consumption and thus to a reduction in greenhouse gas emissions. This is despite the fact that the relationship between land surface temperature (LST, observed by remote sensing) and near- surface air temperature is far from straightforward [14]; and that heat island intensity is greatest at night [15,16], but the effect of vegetation is manifested mostly during the day [17].

Although the mechanisms by which vegetation affects microclimate have been studied extensively, the reported magnitude of the effect of vegetation on meteorological parameters such as air temperature, humidity, wind speed and air quality is quite broad. Vegetation effects on near-surface air temperature, the most reported datum, are usually reported for a specific set of conditions, and thus display a very broad range. Once the change in temperature is normalized by the added surface area of vegetation relative to the total plan area, the resulting efficacy may range from less than 1° [18] to as much as 8° [19]. Although this wide range is partly due to different reporting protocols, much of the variance reflects the huge disparity among locations in terms of the characteristics of the built environment, such as the initial plan area density of the buildings and the street canyon aspect ratio; differences in climate (e.g., tropical vs. desert), and consequently the Bowen ratio; and the properties of the vegetation. Many of the studies compare urban parks with built-up areas [20–22], but the reported differences in temperature relative to built-up areas cannot be realized in practice where vegetation cover is limited by existing buildings. The

Abbreviations: UHI, urban heat island; CCP, climatic cooling potential; LST, land surface temperature; TMY, typical meteorological year; CAT, Canyon Air Temperature model; GIS, geographical information system; SEB, surface energy balance; HVAC, heating, ventilation and airconditioning; ASHRAE, American Society of Heating, Refrigerating and Air-Conditioning Engineers.

* Corresponding author.
E-mail address: erell@bgu.ac.il (E. Erell).

results of studies on microclimate modification by vegetation are also frequently misinterpreted by the planning community and are applied out of context [23]. However, the growing number of cities that have adopted policies supporting extensive planting of vegetation in existing neighborhoods underlines the near universal belief in the beneficial effects of vegetation.

Much of the recent research into the effects of adding vegetation to urban neighborhoods at the pedestrian and building scale has been conducted by computer simulation, primarily ENVI-met. ENVI-met is a three-dimensional grid-based computational fluid dynamics (CFD) model [24]. ENVI-met was designed to support detailed modelling of vegetation effects on primary meteorological parameters including air temperature, humidity, and wind speed, and (in later versions) to employ them to estimate complex indicators of human thermal comfort such as the mean radiant temperature (Tmrt) [25], the Physiologically Equivalent Temperature (PET) [26,27] and the Universal Thermal Climate Index (UTCI) [28]. ENVI-met has been used to evaluate the effect of vegetation in numerous urban scenarios [12,29–33]. However, although ENVI-met simulations are useful in scenario testing, they do not generate inputs required for detailed building energy modelling, since they are limited in time to very short periods, typically 24–48 h.

Building energy simulation is performed using software that describes building characteristics and in some cases equipment, typically over an annual cycle [34]. Such software requires co-temporal hourly values of various meteorological parameters in the form of a Typical Meteorological Year (TMY), which is derived from long-term weather records at a station in the region [35]. TMY files, which are used for engineering design and regulatory purposes, are available for numerous locations worldwide (e.g., US DOE, 2018). They are an accurate representation of the conditions at the weather station, which is typically at an airport location – but not at the heart of the built-up area, where the building might be located. Because TMY files are based on data for specific locations, they cannot be used as-is for scenario testing in conditions other than those for which they were assembled. Generating 'urbanized' TMY files as inputs for building energy simulation was proposed by Erell and Williamson [36] in the CAT model and Bueno et al. [37] in the Urban Weather Generator (UWG), but with few exceptions (e.g. Crawley) [38], this approach has not been implemented widely in practice.

Intra-urban variability of microclimate may be substantial [39–41]. This is primarily due to the diversity of urban form, as expressed in building height and density, land use and land cover (LULC) and construction materials, so that rather than referring to a location as either 'urban' or 'rural', there is in fact a continuum of local climate zones (LCZs) [42]. Correspondingly, the effects of vegetation differ according to city size, geographical location and local climate [43]. Since a given intervention may result in different outcomes in different locations, decisions on policy need to be evaluated on the basis of local data. Despite progress made in modelling urban climate, simple tools are not readily available for urban planners to assess the climatological impact of different development scenarios, including increasing vegetation cover [44]. Additionally, the complexity of the urban planning process and the large number of experts and stake holders involved in any development project make it extremely difficult for the climatologist to make a meaningful contribution to the design [45,46]. The localized climate data for building energy simulation could in theory be provided by modelling the urban climate, and there has in fact been progress in this field, summarized in a thorough review by Lauzet et al. [47]. However, despite this progress, Mills' observation [48] that in practice, these are separate disciplines, pursued by different communities with little interaction, remains largely true. Building certification in the construction industry does not require, or even recognize, modelled climate data at the urban scale. Concurrently, most academic studies of the effect of urban greening on building energy consumption simply assume that lower air temperature, especially during the warm daytime hours, will necessarily lead to savings, or use simplified methods to estimate its effect.

Urban greening can take many forms: vegetation may be found on buildings (green roofs or green facades), on building lots, along streets, or in urban parks and gardens [49]. The effect of vegetation on building energy consumption may be complex [50], with seasonal variations depending on the local climate. Interactions between plants, such as trees shading grass, affect both the energy balance and water consumption [51]. A comprehensive analysis of all possible outcomes is beyond the scope of one study. Most previous studies have focused on the contribution of vegetation to heat island mitigation, with several incorporating a methodology to include the spatial scale of the intervention, typically for specific weather conditions or time of day [52,53]. The present study seeks to assess the overall *annual impact* of plants, focusing on surface cover vegetation such as grass, while acknowledging that trees, for example, may provide greater benefit – but are far more complex to model on this time scale.

This study has two objectives:

First, to demonstrate the importance of using appropriately urbanized weather files to provide detailed and realistic site-specific building energy consumption estimates through computer simulation. Although such studies have been performed by means of a building energy model (BEM) incorporated in an urban climate model, such as WRF [54–56], the primary purpose of the method was to accurate estimations of the urban heat island (air temperature and anthropogenic heat fluxes), and it is used for regional scale urban climate simulations. The emphasis here, in contrast, is to improve the building energy model by providing urbanized climate data that incorporates effects such as the urban heat island, which are then used as inputs to EnergyPlus, which is a software tool developed to perform accurate building energy simulations. The only tools used for annual simulations of the urban climate for use in building energy models [47] are the parametric tools UWG, CAT and CIM, though CIM [57] is a large-scale model and its meshing is not suitable for analyzing the impact of local adaptation strategies. Parametric energy balance models are best suited for generation of urbanized weather data for building energy simulation since they can generate hourly data for an entire year. While this approach has been demonstrated by Erell & Williamson [58] and Bueno et al. [37], it has thus far been implemented in a very small number of studies, especially regarding the effects of vegetation.

Second, to present a methodology for assessing the impact of increasing vegetation cover in existing urban areas on building energy consumption and to estimate the magnitude of the energy savings in residential buildings in a Mediterranean city. Almost all the studies on this topic have been performed using ENVI-met, which provides very detailed modelling of the effects of vegetation. However, ENVI-met is limited to short time periods of 2 days at most and does not simulate actual building energy consumption directly at all, the assumption being that if air temperature is lower, cooling requirements will be lower, too. A literature review found no studies in which an urban weather generator was used to simulate the effect of vegetation on the urban microclimate at an hourly resolution for an entire year to generate a modified weather file, which is then used for an annual simulation of energy consumption using a dedicated building energy software such as EnergyPlus.

2. Methodology

The study employs computer simulation to predict the microclimate of an urban street canyon, based on measured data from a reference weather station in a rural area. The Canyon Air Temperature (CAT) model [36,59,60] is used to generate modified typical meteorological year (TMY) files for urban street canyons of varying geometry and different vegetation cover. These data are used as inputs for assessing:

1. The 'climatic cooling potential', a metric which is similar to Cooling Degree-Hours but which relates to free-floating (non-air conditioned) buildings.
2. Building energy performance, using ENERGYui [61], a graphic user interface for the EnergyPlus building thermal simulation software (US DOE, 2008). ENERGYui was developed to generate building energy efficiency labels according to Israel standard SI 5282.

Both indicators were calculated first for the reference (rural) weather station at Bet Dagan (32°0′28"N, 34°48′52"E); then for conditions in typical (existing) streets in Ramat Aviv, a suburb on the northern outskirts of Tel Aviv; and finally for different scenarios of plant cover.

2.1. The study area

Tel Aviv comprises the core of Israel's largest metropolitan area and is located on the eastern coast of the Mediterranean Sea. Its climate is classified as Mediterranean (Köppen Csa), with mild, rainy winters and warm and humid summers. It has 530 heating annual degree-days (to 18.3 °C) and 3,810 cooling degree-days (to 10 °C). Base temperatures for HDD and CDD conform to ASHRAE Standard 169 - Climatic Data for Building Design Standards.

The study area comprises the Ramat Aviv neighborhood, about 1.5 km inland from the Mediterranean Sea (32°11′N, 34°79′E). Streets are about 15–25 m wide and flanked by buildings of varying height, from two or three storeys to as much as 16 storeys high. The neighborhood is considered fairly green (by Israeli standards). The albedo of building walls is estimated at 0.4, and the asphalt road surface at 0.15.

Climate data in the form of a TMY (typical meteorological year) were obtained for the Bet Dagan station, about 11.8 km south of the study site. These data, which are used to represent Tel Aviv for the purpose of building energy rating according to SI5282, are also used as the reference data in this study.

Fig. 1 shows satellite images of the study area, with insets of the rural reference station (Bet Dagan) used to force the simulation, the Tel Aviv beach weather station used for validation, and the Ramat Aviv urban

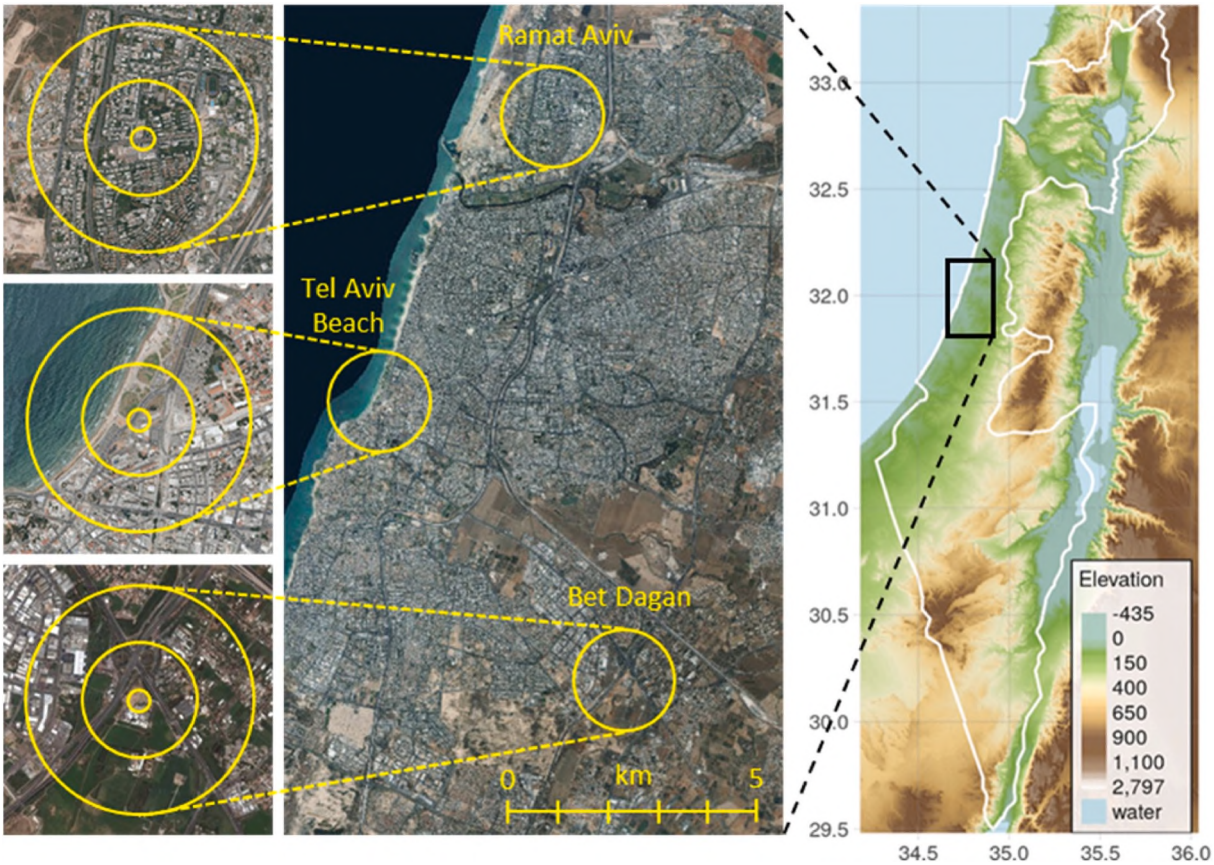

Fig. 1. Location of the study area, showing the Bet Dagan weather station, the Tel Aviv beach station, and the Ramat Aviv neighborhood. Circles indicate radii of 100, 500 and 1,000 m from site. (satellite images: https://www.govmap.gov.il/?c=204000,595000&z = 0).

neighborhood, each with a superimposed matrix for estimating source areas for advected moisture, following Erell et al. [62].

2.2. The Canyon Air Temperature model (CAT) simulation

The CAT model uses meteorological data from a nearby representative weather station to generate time series of local-scale meteorological parameters at an urban street canyon [58]. The transformation is based on a complete surface energy balance at the two sites: In addition to analysis of radiant exchange accounting for short and long-wave fluxes, it incorporates several elements of the LUMPS parameterization scheme [63], including moisture advection from nearby vegetation and bodies of water, as detailed in Erell et al. [62]. The effect of turbulent mixing in different stability regimes is estimated by means of an empirical correlation established using site data from Adelaide and Goteborg and re-evaluated using data from Phoenix. The Canyon Air Temperature (CAT) model applied here is an updated version incorporating effects of soil moisture on the surface energy balance [64]. The CAT model was validated using measurements carried out over an extensive period in Adelaide, and separately using data from an urban canyon experiment in Goteborg, Sweden [65].

The following sections describe subsequent modifications made to the CAT model. A summary of the updated model inputs is presented in Table A1 in the Appendix.

2.2.1. Model inputs

Following Kaplan et al. [59], the urban canyon 3D geometry and land cover information for each street segment can be estimated using GIS data sets and remote sensing. In this study, we divided the neighborhood of Ramat Aviv and its vicinity into a total of 828 (23 × 36) grid cells of 100 × 100 m^2. We further refined the algorithm to derive input variables more efficiently for each grid cell from GIS datasets, as described below. The characteristics of the urban neighborhoods obtained using the methodology described in the following paragraphs are shown in Figs. 2 and 3.

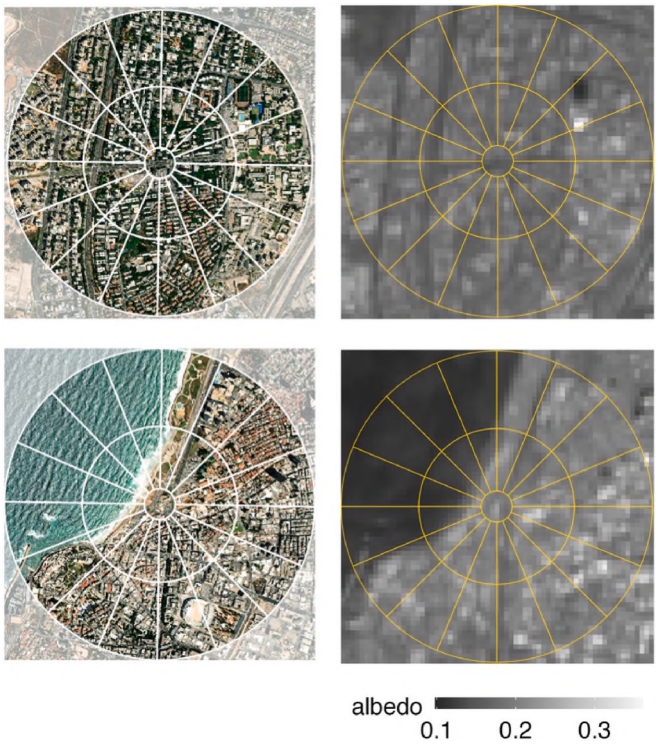

Fig. 2. Optical images (left) and albedo obtained by analysis of satellite images (right) of the two urban sites (Ramat Aviv and Tel Aviv Beach).

2.2.1.1. Albedo. Landsat 8 images are used to estimate the total shortwave albedo with an empirical formula previously developed for the Landsat TM/ETM + sensor [66]:

$$\alpha = 0.356 \times b2 + 0.13 \times b4 + 0.373 \times b5 + 0.085 \times b6 + 0.072 \times b7 - 0.0018$$

Where b2, b3, b4, b5, b6 and b7 correspond to the reflectance in Landsat-8 spectral bands 2 (0.45–0.515 μm), 3 (0.525–0. 60 μm), 4 (0.63–0.68 μm), 5 (0.845–0.885 μm), 6 (1.560–1.660 μm) and 7 (2.1–2.3 μm), respectively. This empirical formula was previously validated using ground measurements of several land cover types in Maryland, USA and archived a residual standard error of 0.019, and R^2 of 0.841 [67]. The albedo data derived from the 30 × 30 m^2 Landsat images are then disaggregated to 1 × 1 m^2 using the nearest neighbor method while masking the building footprints. The mean albedo for each 100 m grid cell is calculated by averaging all ground albedos within it. The mean albedo values of the cells in the area analyzed range from 0.10 to 0.31.

2.2.1.2. Land use and land cover fraction. CAT requires a detailed description of vegetation and water fractions in each grid cell and its vicinity to account for the advection of moisture from source areas that are defined by wind direction and stability [62,65]. Vegetation fraction is estimated from Sentinel-2A[1] images at 10 m resolution using a supervised classification and regression trees (CART) classifier [68], trained by data collected using Google Earth images. The classifier achieved an overall accuracy of 0.98 and identified 4 land use/land cover classes: roads, buildings, exposed soil, and vegetation.

The vicinity of each cell is partitioned into 32 wedges around it, based on pre-assigned azimuths and distances relative to the cell center: 16 pie-shaped slices of 22.5° per each are further divided into 2 concentric segments at distances of 100–500 m and 500–1000 m away from the grid cell center. The vegetation fraction of each wedge is calculated based on the gridded land use/land cover map generated above. For an illustration of the configuration of wedges, we refer to Ref. [59].

2.2.1.3. Urban geometric variables. The CAT simulation requires a description of the geometry of urban street canyon, i.e., building height, street width and orientation, to account for the energy balance. The derivation of those variables requires a spatially explicit GIS database describing building footprints, street networks, etc. The estimation of variables was conducted using the R software [69], and ArcGIS 10.6 [70].

Street width: Using the building footprint layer as input, a grid of 1 × 1 m^2 resolution raster cells is generated, which gives the distance from each raster cell to the closest building. The distance raster reaches its local maximum along the center line between any two adjacent buildings. The set of local maxima constitutes the de facto urban streets. As the distance represents only half of the street, the real street width is double the local maximum. Considering the site-specific street characteristics, we introduced a minimum threshold of 10 m, i.e., only linear spaces wider than 10 m are regarded as streets. The street width of a grid cell is averaged over all streets within it. Given that an urban street canyon (defined for the purpose of microclimatic analysis) can be formed even if there are no discernible paved roads between adjacent building blocks, our approach is capable of robustly describing urban geometry in a systematic way. For more details, please see Zhou et al. [71].

Street orientation: The street orientation (azimuth) is determined based on the de facto urban streets delineated above. We specified 0° for the north. Each link (edge) of streets in a grid cell is projected onto the

[1] Sentinel-2A sensors: https://www.satimagingcorp.com/satellite-sensors/other-satellite-sensors/sentinel-2a/.

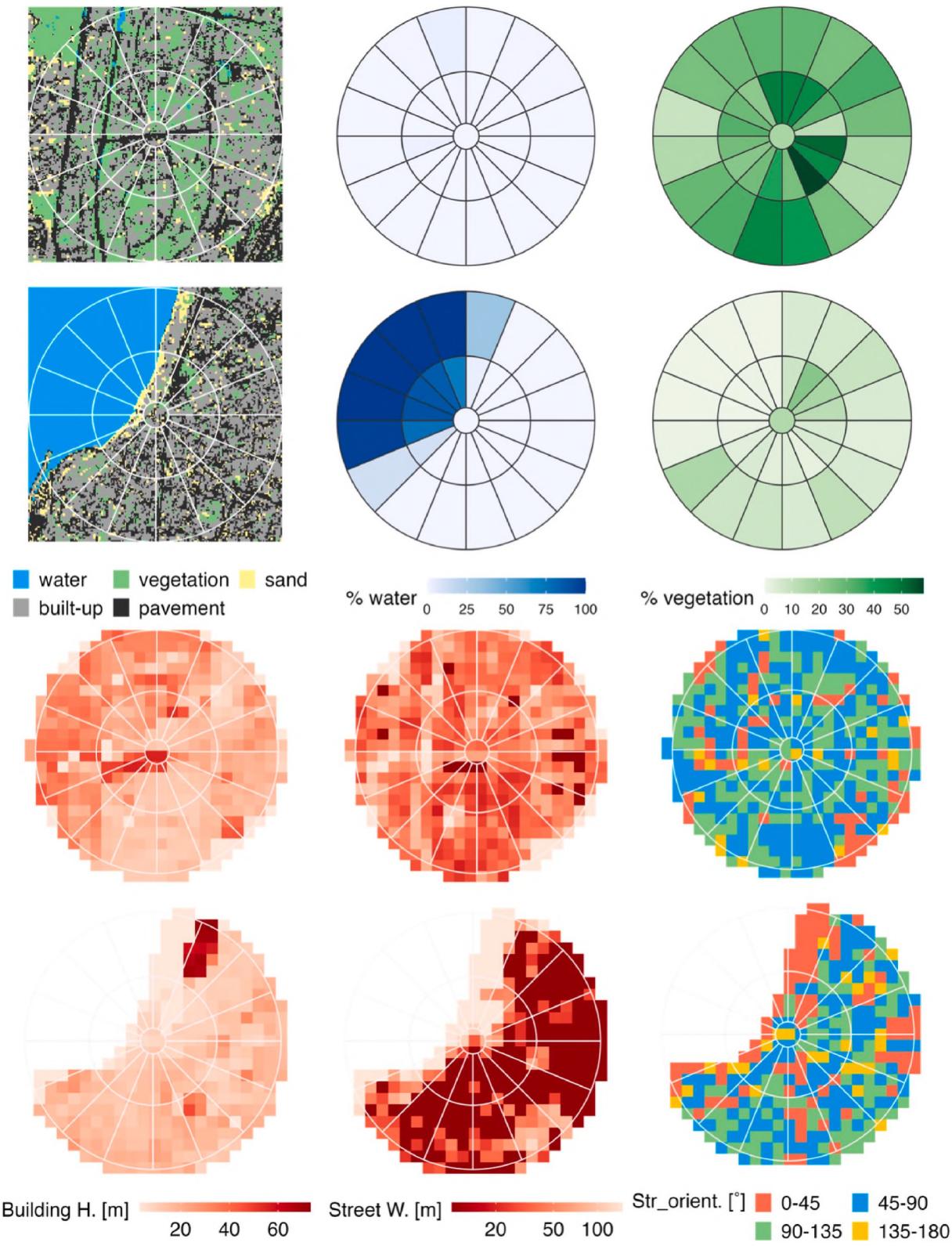

Fig. 3. Characteristics of the two urban sites (Ramat Aviv and TA Beach): Surface cover (above) derived from satellite images, and urban geometric variables of the built fabric (below), derived from a GIS database.

cardinal directions. However, due to the symmetry of the street orientation, we restricted the orientation angle to 0–180°. The street orientation of a grid cell is the vector sum of street vectors within it.

Building height: For each grid cell, the mean building height is calculated by averaging the heights of all buildings within it, weighted by their wall areas. For grid cells free of buildings, i.e., open space, we set the building height to a value of 3 m and the street width to 150 m, which corresponds to a sky view factor of 0.99.

2.2.1.4. Anthropogenic heat. The urban surface energy balance (SEB) includes anthropogenic heat, primarily heat lost from buildings and from vehicle traffic. The CAT model accounts for differences in emissions among neighborhoods of different density, at hourly time steps. For a detailed description please see the SI in Zhou et al. [71]. Heat transfer from buildings is estimated as steady-state conduction through facades using typical thermal properties of walls and windows, assumed to be proportional at each time step to the difference in air temperature between the building interior (assigned according to a seasonal schedule) and exterior. Sensible heat loss by convection is estimated assuming a fixed number of air changes per hour between the interior and the exterior, based on the construction quality and airtightness of fenestration. In summer, sensible heat ejected by air conditioners is assumed to be proportional to the difference in air temperature between the interior and exterior. A detailed description of the building energy model and simulation parameters is given in Section 2.5 and Tables A2 and A3 in the Appendix.

Heat emitted by automobiles is estimated as the product of the heat emitted by a typical car – 3,795 J/m [72] and the number of vehicles travelling down the street. A simplified procedure, which is necessarily crude, assigns automobile traffic at a given location based on street width (broad streets have higher traffic) and diurnal load. The estimated vehicle count at hourly intervals is given by multiplying the capacity of the street by a traffic fraction that describes a typical diurnal profile with morning and afternoon peak traffic and a very small number of vehicles at night [72].

2.2.2. CAT model validation

Typical Meteorological Year (TMY) files contain concurrent values of meteorological variables at hourly intervals for an entire year. The objective of the CAT simulation is to generate 'urbanized' TMY files representative of specific locations or scenarios, so model validation requires time series describing long periods and varied weather conditions in different seasons – preferably for an entire year. In the absence of a suitable weather station providing such data for Ramat Aviv, model validation was performed using data from a weather station located within the urbanized area, several kilometers south of the Ramat Aviv neighborhood. As in the case of simulations conducted to test various scenarios in Ramat Aviv, the simulations were forced by weather data from the Bet Dagan weather station operated by the Israel Meteorological Service, for the entire 2016 calendar year.

Statistical measures of model performance are shown in Table 1.

Because air temperature at the urban site is very similar to air temperature at the reference weather station that is used as a model input, simple regression analysis does not provide a satisfactory test of model performance. The model may only be considered useful if the simulation output is closer to the observed value than this input. This may be assessed by the Williamson Degree of Confirmation [73], which may vary from $-\infty$ to 1.0, with values between 0.0 and 1.0 indicating an improvement relative to using the unmodified weather station data. Nevertheless, it is useful to also review conventional indicators such as the mean error and root mean square error (RMSE).

Table 1
Statistical evaluation of the predicted air temperature, for 2016.

Total number of hours	8760
Mean error (°C)	0.08
Standard deviation of error (°C)	1.64
Root mean square error (°C)	1.64
Systematic root mean square error (°C)	0.35
Unsystematic root mean square error (°C)	1.60
Willmott index of agreement	0.98
Williamson degree of confirmation	0.329

Fig. 4a–d and 5a-d illustrate model performance for winter (January) and summer (July), for air dry bulb temperature and relative humidity, respectively. Fig. 4a (top) shows temperature evolution over a period of 7 days in winter, beginning with dry sunny weather followed by cooler overcast weather. Fig. 4b shows a 7-day summer period, with warm dry weather typical of this Mediterranean location. Fig. 4c and d shows ensemble diurnal patterns for each month, representing the mean hourly values over 31 days in the respective months. Similarly, Fig. 5a–d shows the evolution of relative humidity for the same periods.

2.3. Climatic cooling potential

In addition to assessing the urban effect on energy consumption for heating and cooling, it may also be evaluated in terms of its effect on buildings that do not have air conditioning, or where owners prefer to minimize its use by maximum utilization of so-called 'free cooling' by night ventilation. The metric selected for this assessment, the 'climatic cooling potential' (CCP) proposed by Artmann et al. [74], is an artificial metric that allows comparison of the potential for cooling by ventilation in a non-air-conditioned building. Rather than prescribing a fixed reference temperature for cooling, as is done in the calculation of the Cooling Degree Days metric, this method assumes that internal building temperature is allowed to oscillate harmonically in response to the diurnal cycle of external air temperature, with a time lag and decrement factor that are due to the presence of thermal mass in the building fabric. For this analysis, the building (reference) temperature at time h is given by the expression:

$$T_{b,h} = 24.5 + 2.5 \cos\left(2\pi \frac{h - h_i}{24}\right) \quad (1)$$

and h_i is the time ventilation normally starts (for example at 19:00).

Following Artmann, the climate cooling potential (CCP) is defined as

$$CCp = \frac{1}{N} \sum_{n=1}^{\sum} \sum_{h=h_i}^{\sum} m_{n,h} \left(T_{b,n,h} - T_{e,n,h}\right) \quad (2)$$

Where $T_{b,n,h}$ is the building temperature at hour h and $T_{e,n,h}$ is the external temperature at the same time. The difference is summed over a total period of N hours accounting for the value of m, as follows:

$$\begin{cases} m = 1 \text{ if } T_b - T_e \geq \Delta T_{crit} \\ m = 0 \text{ if } T_b - T_e < \Delta T_{crit} \end{cases}$$

As a certain temperature difference is needed for effective convection, Artmann et al. [74] proposed that night ventilation is only applied if the difference between building and ambient temperature is greater than $\Delta T_{crit} = 3$ K. We have adopted a slightly smaller value here ($\Delta T_{crit} >$

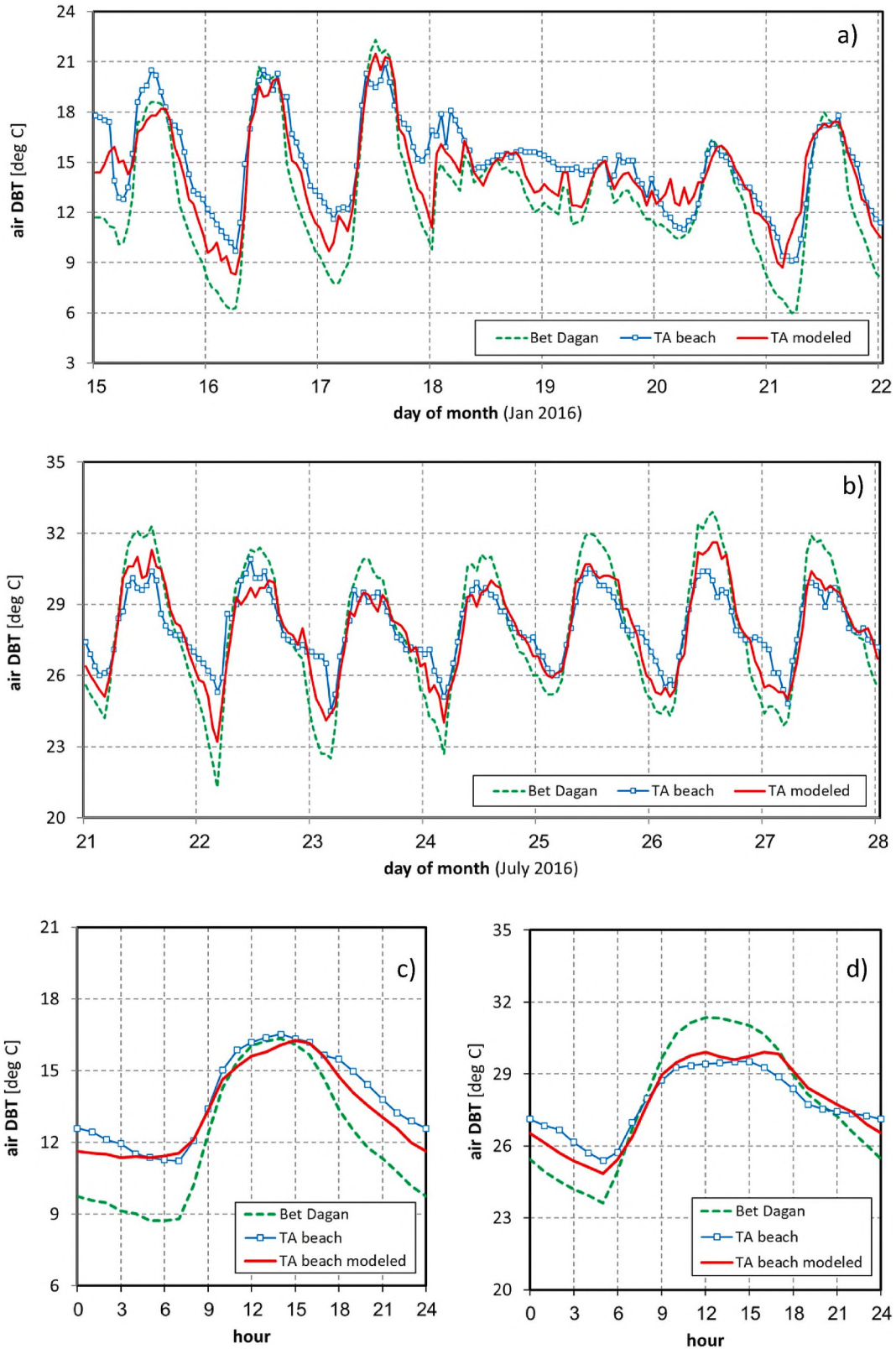

Fig. 4. Time series showing CAT model performance – air dry bulb temperature: a) 7-day period in winter; b) 7-day period in summer; c) ensemble diurnal pattern for January; d) ensemble diurnal pattern for July.

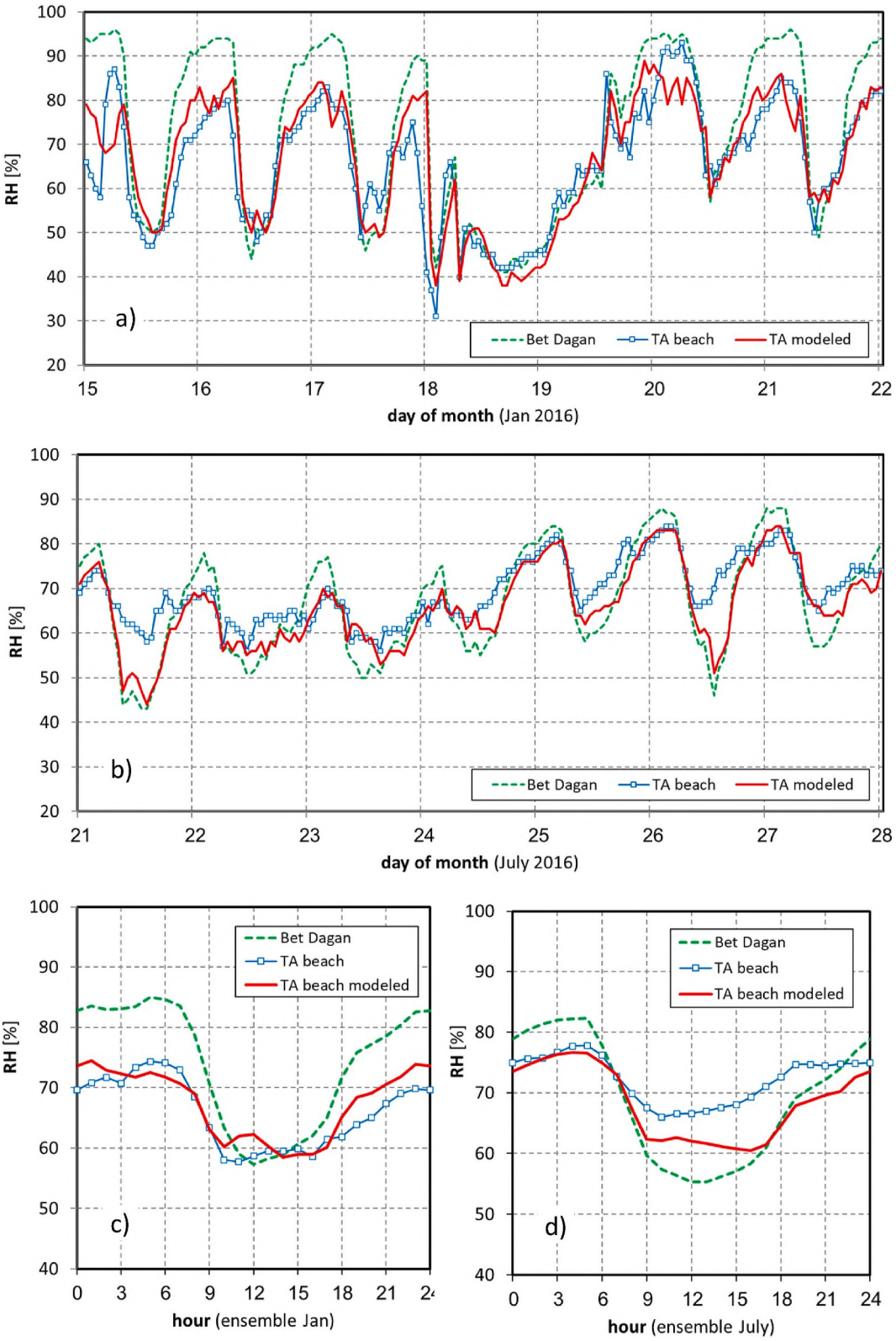

Fig. 5. Time series showing CAT model performance – relative humidity: a) 7-day period in winter; b) 7-day period in summer; c) ensemble diurnal pattern for January; d) ensemble diurnal pattern for July.

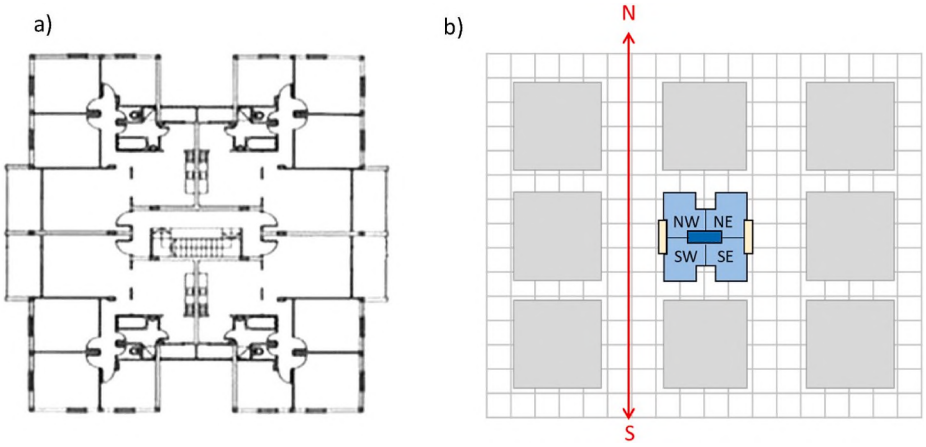

Fig. 6. Building model. a) Typical floor plan. b) Modelling shading by adjacent buildings in ENERGYui, for a 'N–S street' scenario. (Polygons shaded in grey represent volumes of adjacent buildings that EnergyPlus treats as non-climatized spaces.). (For interpretation of the references to colour in this figure legend, the reader is referred to the Web version of this article.)

2 K), since a larger value might result in elimination of the cooling potential assessed by means of the metric entirely, while night ventilation is in fact employed extensively in Tel Aviv.

2.4. EnergyPlus and ENERGYui

EnergyPlus (US DOE) simulates a building's thermal load based on a description of its physical make-up and mechanical systems, as well as solar exposure and meteorological data. The program calculates heating and cooling loads necessary to maintain a user-specified temperature or temperature range. EnergyPlus is an extremely flexible and capable simulation tool [34]; it provides a detailed breakdown of consumption according to sources; and it is accepted as an aid in demonstrating compliance for numerous green building standards including LEED and BREEAM.

ENERGYui [75] is one of several graphical user interfaces for EnergyPlus. It compares thermal loads of simulated residential or office buildings with the Israeli Standard 5282 - Energy Performance for Buildings. Outputs are represented as an efficiency rating for the entire building and for each individual apartment, and a breakdown of thermal loads.

2.5. Simulation parameters

A simulation of the building's thermal loads was carried out for several building variants having the same floor plans but representing different standards of construction: a pre-1980 standard building complying with Israel standards for thermal insulation (SI 1045); a 'green' building with the same floor plan but complying with the energy requirements of the Israel green building standard (SI 581); and a building with a curtain wall design similar to some of the new residential construction in Tel Aviv.

The building has an H-shaped floor plan which is very common in Israel (Fig. 6a). It comprises 4 apartments per floor, each of about 84 m^2 in floor area. The window to wall ratios for all facades of the building are about 0.11–0.12, except for the curtain wall variant, which has a window to wall ratio of about 0.3 on the north and south facades. Building properties for the three variants are shown in Table A2 in the Appendix.

ENERGYui simulates self-shading by building elements such as balconies but does not normally account for shading by adjacent buildings. To achieve a more realistic measure of the effects of solar radiation in a densely built urban neighborhood, a non-climatized built space was added to the model, representing the volume of eight adjacent buildings surrounding the object of the simulation (Fig. 6b). The height of these buildings is assumed to be equal to the height of the simulated building.

The impact of outdoor microclimate on building energy demands was defined as the difference between energy simulation results using the standard TMY weather data (for the Bet Dagan weather station) and results using a TMY file altered by the CAT model to represent the relevant urban scenario and building variant.

2.6. Model linkage and study flowchart

The overall study design is summarized in a flow chart, which also illustrates the sources of data required to run CAT and the coupling between the CAT model and EnergyPlus (Fig. 7).

As the flow chart indicates, CAT is first run to generate 'urbanized' TMY files for each of three scenarios: 1) An actual 100 × 100 m grid cell in Ramat Aviv, accounting for building footprints and heights, surface cover fractions in the cell itself and a 1-km radius area surrounding it, and thermal properties of all canyon facets; 2) The same site, but with surface cover vegetation increased such that it occupies 50% of all non-building areas; 3) The same site, but with all vegetation removed. EnergyPlus is then run, first with the original TMY file based on data from the open reference site, as would normally be done in design practice or for code certification, then with each of the 3 modified versions representing the actual urban site and the two vegetation scenarios. The building energy simulation is performed for each of 3 building types, in two configurations: One with surrounding buildings creating realistic shading on the building, and one with the building being simulated as a stand-alone structure with no adjacent obstructions

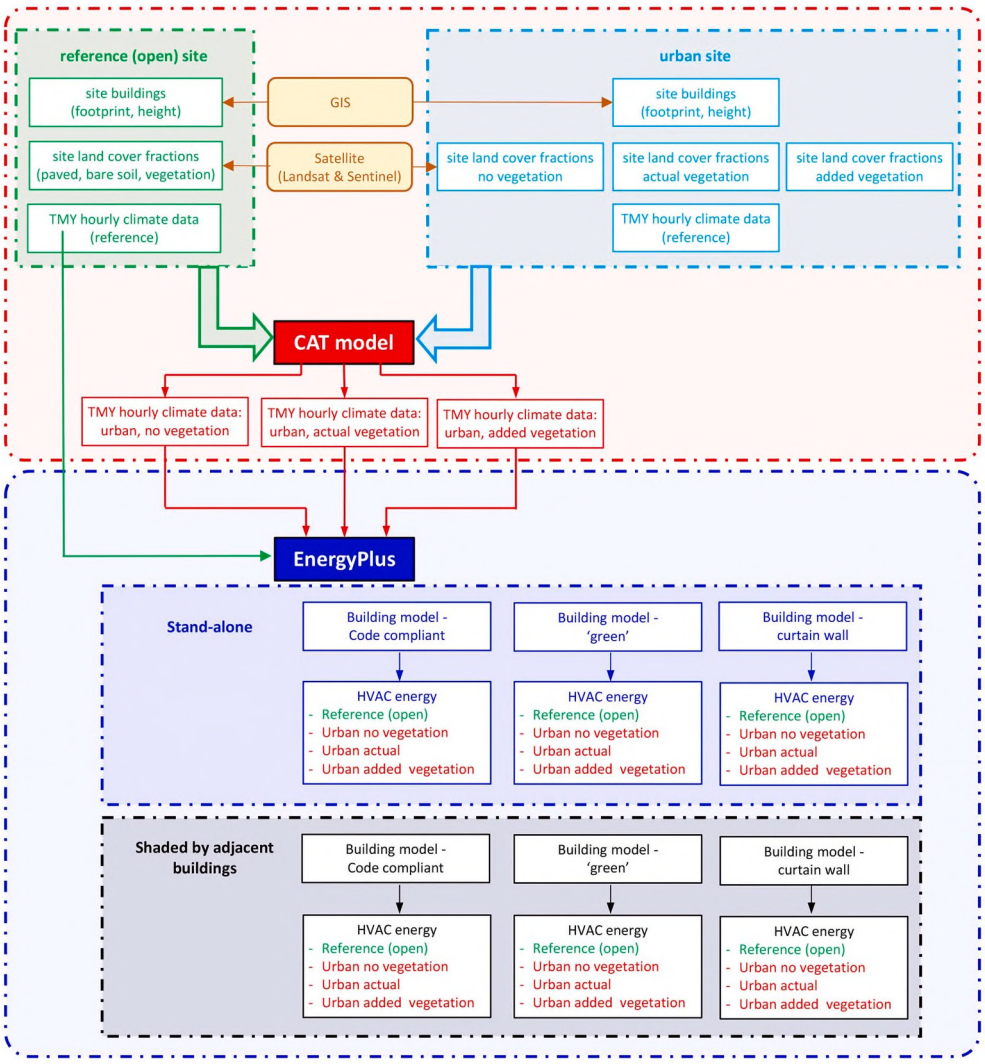

Fig. 7. Study framework.

limiting exposure to solar radiation. There are thus 24 different permutations that allow isolation of the effect on building energy consumption for HVAC of modifying the vegetation cover in the neighborhood, accounting for building characteristics and the effect of shading by adjacent structures.

3. Results and discussion

The following section will first provide results of the street canyon microclimate simulation, followed by an illustration of the impact of the urban modification on the potential for night ventilation and building energy calculations.

3.1. CAT output

The CAT simulation was carried out for 100 × 100 m^2 grid cells for the entire Ramat Aviv neighborhood, using Bet Dagan as the reference site. Fig. 8 shows the UHI intensity simulated by CAT for 04:00 on July 30, 2016. Temperature differences – $\Delta T_{u\text{-}r}$ – reflect the combined effect of variations in surface cover (e.g., vegetation) and geometry (buildings and street canyons) between the Bet Dagan weather station and the suburb of Ramat Aviv. Simulated weather data from two grid cells were selected as inputs for the building energy simulation: The cell highlighted in red, which was identified as a local 'hotspot', and the cell highlighted in green, a neighborhood park where UHI intensity was

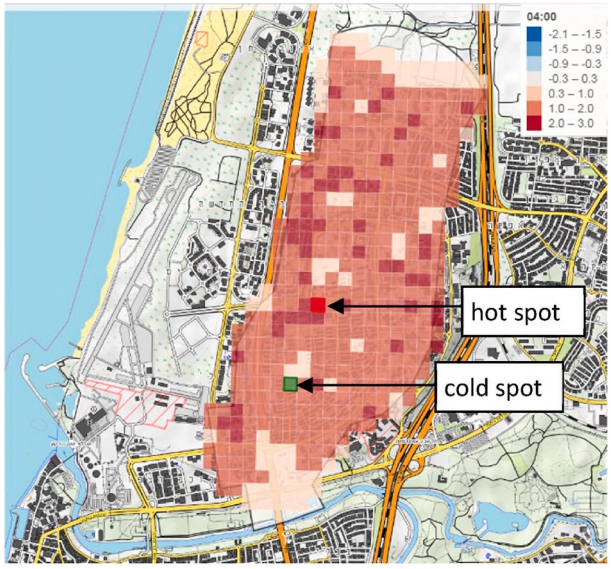

Fig. 8. Ramat Aviv UHI simulated by CAT for 04:00 on July 30, 2016.

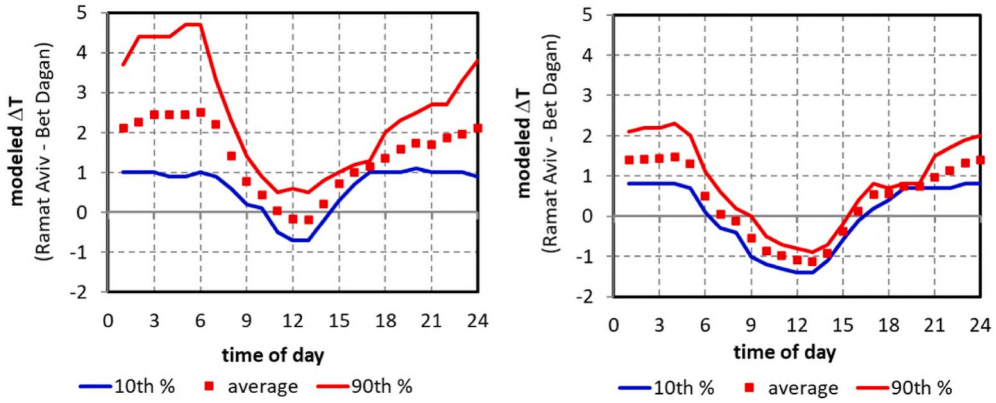

Fig. 9. The modelled diurnal pattern of the UHI in Ramat Aviv, calculated from the urbanized TMY file. Left - winter (January); Right – summer (July).

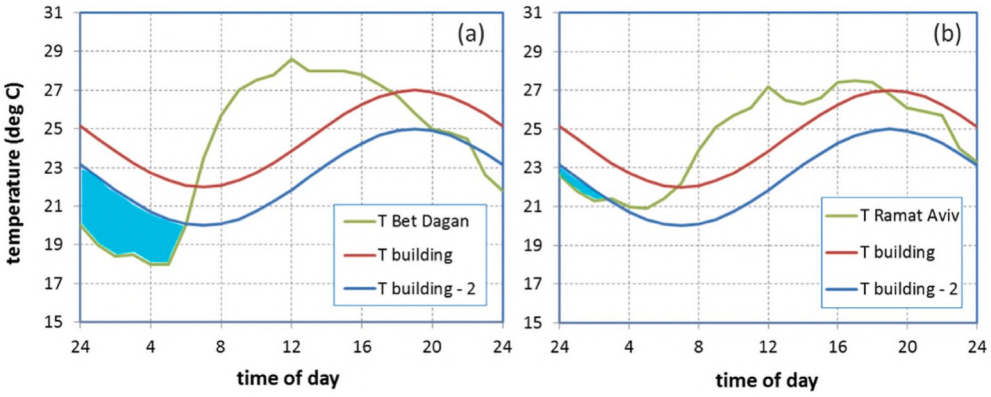

Fig. 10. Hourly air temperature outdoors, indoors and the limit for effective cooling ($T_{building\ -2}$), on a typical day in July. The CCP is represented by the shaded area above $T_{Bet\ Dagan}$ and below $T_{building\ -2}$. a) for an exposed building at Bet Dagan; b) for a building in the Ramat Aviv 'hotspot', using air temperature generated by CAT. The shaded area (cyan) represents the CCP. (For interpretation of the references to colour in this figure legend, the reader is referred to the Web version of this article.)

lowest.

The simulated UHI intensity (illustrated here for the hotspot indicated in Fig. 8 by a red outline) has a clear diurnal pattern (Fig. 9): It is most marked at night, reaching a maximum after midnight, but is weak or even slightly negative during daytime. The urban heat island also has a seasonal pattern, and is stronger in winter than in summer, as well as displaying a greater variance, as indicated by the values for the 10th percentile and 90th percentile of hours. The intensity of the UHI in winter is attributed to lower humidity and clear sky conditions, as well as slightly larger anthropogenic heat related to building space heating.

3.2. *The climate cooling potential*

The effect of elevated night-time air temperature in Ramat Aviv is reflected in the values of the climate cooling potential (CCP). Fig. 10 illustrates the effect of the urban fabric on the climate cooling potential for a typical day in July. In Fig. 10a, the cooling potential is represented by the shaded area between the assumed indoor temperature minus 2° ($T_{building\ -2}$), shown by the solid blue line, and the actual air temperature at Bet Dagan ($T_{Bet\ Dagan}$). The increase in night-time air temperature predicted by the model for the urban location, in Fig. 10b, results in nearly complete elimination of the potential for passive cooling by ventilation during the night in question.

The cumulative effect of changes to the CCP over an extended summer period is demonstrated for the months of July and August. In Bet Dagan, the total cooling potential for the two-month period is 1,738 degree-hours. The comparable value for the vegetated area in Ramat Aviv is slightly smaller: 1,519 degree-hours. However, at the local hotspot the cooling potential is almost entirely eliminated: only 345 degree-hours.

The difference between the potential for night ventilation in the reference condition (used in SI5282 for labelling building energy performance) and a more realistic urban condition is striking. This difference is the result of the compound effects of vegetated surface cover and of increased urban density and is certainly far too large to ignore either in system design or in the building certification process.

3.3. *Building energy simulation*

3.3.1. *Effect of environmental exposure*

The energy consumption of a building is affected by the environmental conditions to which it is exposed. These are normally described by the hourly meteorological data and by the concurrent solar radiation fluxes. Based on the date and geographic location, solar altitude and azimuth may be calculated for every time step, supporting shading studies, but building codes and rating schemes rarely require calculation of the effect of shading by adjacent buildings, so that performance is often simulated for the building in isolation. The effect of solar exposure varies according to climate and the specific design of the building, in particular the size and orientation of glazed areas.

Table 2 shows the modelled annual energy demand for the three variants of an 8-storey building (see Table A2 in the Appendix), first for

Table 2
Simulated annual heating and cooling demand for 3 types of 8-story buildings in each of 3 climate scenarios, for a stand-alone building and for a building shaded by adjacent structures.

	Bet Dagan	Ramat Aviv green		Ramat Aviv canyon	
	kWh/a	kWh/a	% change	kWh/a	% change
stand-alone					
standard	50,052	46,176	−7.74	48,890	−2.32
green	48,674	44,835	−7.89	47,132	−3.17
curtain wall	53,409	49,958	−6.46	53,287	−0.23
shaded					
standard	54,689	49,754	−9.02	51,090	−6.58
green	46,975	42,979	−8.51	44,636	−4.98
curtain wall	49,238	45,548	−7.49	48,012	−2.49

an isolated 'stand-alone' building exposed to urban climate scenarios investigated (Bet Dagan as the reference weather station, the green site in Ramat Aviv simulated by CAT, and the urban canyon in Ramat Aviv, also simulated by CAT), then for the same building affected by shading from adjacent structures for each of the three climate scenarios.

As the table shows, energy consumption for heating and cooling is affected firstly by building characteristics: the 'standard' building requires substantially more than the 'green' building in all scenarios.

Exposing each of the three building types to the climate of the open green space in Ramat Aviv results in a substantial reduction in the HVAC demand, reflecting the difference between Bet Dagan, which is several kilometers inland, and Ramat Aviv, which is closer to the Mediterranean Sea. However, when exposed to realistic urban conditions (Ramat Aviv street canyon), there is a noticeable increase in simulated energy consumption relative to the open space, for all building configurations.

When the effect of shading by adjacent buildings is incorporated in the simulation, the effect of the urban street canyon on energy consumption, though still present, is somewhat moderated.

As this analysis makes clear, there are substantial variations in environmental conditions, even within a relatively small area such as the Tel Aviv metropolitan region, which are reflected in the simulated energy demand for building heating and cooling.

Table 3
Simulated annual heating and cooling demand for 'standard' 8-story building shaded by adjacent structures, using Bet Dagan data and an urbanized TMY data file generated by CAT.

	electricity consumption (kWh)			electricity use intensity (kWh/m^2)		
	heating	cooling	total HVAC	heating	cooling	total HVAC
Bet Dagan	20,053	34,636	54,689	7.4	12.8	20.3
Ramat Aviv canyon	10,587	40,503	51,090	3.9	15.0	18.9
diff (kWh)	−9,466	5,867	−3,599	−3.5	2.2	1.3
diff (%)	−52.8	16.9	−6.6	−52.8	16.9	−6.6

3.3.2. *Seasonal effects*

To understand why the difference in total annual energy consumption for all of the building types is fairly modest in comparison to the impact of urban effects on the Climate Cooling Potential, the energy consumption was further broken down by season.

Table 3 shows the total annual energy consumption for heating and cooling of the standard 8-story building described above, accounting for shading by adjacent buildings. As the table shows, the urban heat island causes a reduction in winter heating demand in the urban area, compared with the rural Bet Dagan station. This is offset by a substantial increase in summer cooling loads, resulting in a net decrease of about 6.6% in the total energy consumption for heating and cooling.

3.4. *The effect of increasing plant cover*

The effect on microclimate and building energy consumption of adding surface cover vegetation was simulated using CAT to generate modified weather files (.epw) for the ENERGYui simulation. Three scenarios were investigated: A local intervention, in which the vegetation fraction of the urban canyon site within a 100 m radius of the center of the grid cell was increased from the existing 12% to 50%; a neighborhood-scale intervention in which the vegetation fraction of the entire area within a 1 km radius of the representative canyon site was increased to 50%; and a contrasting scenario in which all existing vegetation in the neighborhood was removed. In both vegetated cases, the vegetation modelled comprised surface cover plants such as grass, which affects the surface energy balance through evapotranspiration and direct radiant exchange at the surface, but not by shading (i.e. not

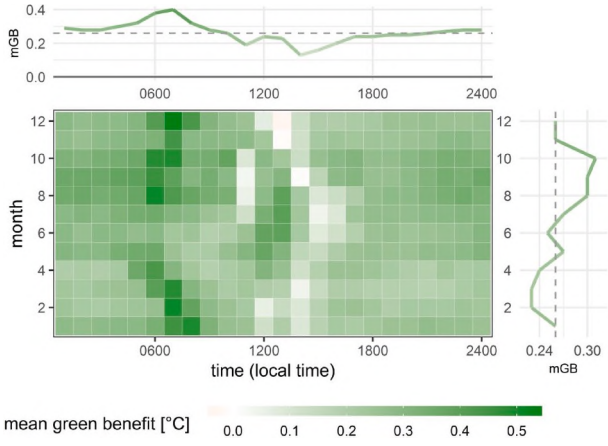

Fig. 11. Simulated temperature reduction due to increasing green surface cover in the Ramat Aviv street-canyon. The horizontal time series (top) shows mean hourly values, and the rotated vertical time series graph (right) shows mean monthly values. Note that positive values indicate a 'benefit', i.e. a cooling effect. (For interpretation of the references to colour in this figure legend, the reader is referred to the Web version of this article.)

Table 4
Simulated effect of green surface cover on annual heating and cooling demand for 8-story building shaded by adjacent structures, using urbanized TMY data files generated by CAT for current street canyon and the same grid cell with *50% green* surface cover.

	Ramat Aviv canyon (kWh/a)			Ramat Aviv green canyon (kWh/a)			Difference	
	heat	cool	total	heat	cool	total	kWh/a	%
standard	10,587	40,503	51,090	11,681	38,048	49,729	−1,361	−2.66
green	7,531	37,106	44,636	8,414	34,968	43,382	−1,254	−2.81
curtain wall	5,779	42,234	48,012	6,540	40,104	46,645	−1,368	−2.85

Table 5
Simulated effect of green surface cover on annual heating and cooling demand for 8-story building shaded by adjacent structures, using urbanized TMY data files generated by CAT for the current street canyon and for the same grid cell (and source areas for advection within a 1 km radius) with *no green* surface cover.

	Ramat Aviv canyon (kWh/a)			Ramat Aviv no green canyon (kWh/a)			Difference	
	heat	cool	total	heat	cool	total	kWh/a	%
standard	10,587	40,503	51,090	9,935	41,930	51,865	775	1.52
green	7,531	37,106	44,636	7,009	38,363	45,371	735	1.65
curtain wall	5,779	42,234	48,012	5,340	43,487	48,826	814	1.69

trees). The green area was assumed to be well-watered, such that when soil moisture levels modelled by CAT dropped (through evapotranspiration) to 0.05 they were increased by the software to 0.25 (thus implementing irrigation), sufficient to support unrestricted evapotranspiration from plants.

The effect of adding vegetation is first observed in the surface energy balance. As may be expected, adding vegetation increases the latent heat flux and leads to a corresponding decrease in the sensible heat flux during the hot daytime hours in summer, resulting in lower air temperature (see Supplementary Information for further details). The CAT simulations showed that the effect of both green interventions on air temperature was very similar: Relative to the existing street canyon, increasing plant cover led to an average annual temperature reduction of about 0.25 °C, with a maximum reduction of 3.2 °C. The largest effect predicted by the simulations was in the early morning (between 6 and 9 a.m.) on winter days (Fig. 11). Daytime cooling in summer, when it is most needed, is modest, ranging from 0.2 to 0.5 °C for 90% of the time.

The air temperature modification induced by the added vegetation led to a small reduction in the simulated annual energy demand for heating and cooling in all 3 building types (Table 4). Lower air temperature led to slightly larger heating loads in winter, but this was more than offset by reduced demand for air conditioning in summer. On balance, the simulated energy saving is equal to about 2.5–3% of the initial energy expenditure.

As expected, simulations show that removing existing vegetation has the opposite effect: The mean annual air temperature will increase by about 0.42 °C. This temperature increase is reflected in the simulated energy demand: heating demand is expected to decrease, while demand for air conditioning is projected to increase, more than offsetting the winter savings (Table 5). The balance, an increase of about 1.5–1.7%, is a measure of the benefit of current vegetation in the neighborhood.

4. Discussion

The method described in the present study accounts for the effects of vegetation on air temperature and humidity, which are incorporated into the urbanized weather file. CAT models radiant fluxes from each of the urban facets explicitly, including reflected solar radiation and long wave radiation emitted from all canyon surfaces. To establish the temperature of each building facet, CAT also models wind speed adjacent to the surface, based on measured values at the reference station that are transformed to account for urban boundary layer effects and in-canyon vortex flow. However, EnergyPlus assigns all such surfaces a temperature that is equal to the prevailing air temperature (Engineering Reference, EnergyPlus V. 8.0), and calculates long-wave radiant exchange with surrounding surfaces accordingly. The net effect of modifying a fraction of the surface from pavement to vegetation on the radiant flux emitted by the ground and absorbed by building surfaces in a dense neighborhood with tall buildings will be small, because the view factor calculated from each building façade element to the patch of vegetation, perhaps several floors below, will be very small. If the ground surface in question is also shaded by adjacent buildings, then the difference will be even smaller. The effect on wall surface temperature and hence on annual building energy consumption will, in this context, be correspondingly small.

Since the study is limited to surface cover vegetation, such as lawn or low bushes, it does not account for potential benefits from shading buildings, such as could be obtained from trees. However, unlike detached low-rise buildings, the contribution of shading to the reduction of cooling demand in medium-rise or high-rise buildings is necessarily smaller because trees shade only the lowest floors of the building. Their effect is further reduced because the ground floor of such buildings is (at least in Israel) devoted to functions such as a lobby, and not apartments. Finally, if the canyon aspect ratio is large (H/W > 1), then buildings are often shaded by their neighbors, and the additional shade provided by trees is small.

Buildings are a major source of anthropogenic heat. Because buildings and the urban canopy layer are linked, such that meteorological conditions affect building energy consumption, while buildings affect their adjacent environment, an accurate estimate of this process requires an iterative process in a fully two-way coupled simulation. A coupling of EnergyPlus and the TEB model has in fact been demonstrated by Bueno et al. [76]. However, it is impractical, since it requires not only very extensive computing resources, but also detailed descriptions of the thermal properties of all surrounding buildings within a 1,000-m radius (which is the source area the CAT model considers). Consequently, later versions of this methodology, such as Bueno et al. [37], have reverted to offline, one-way coupling of a building energy model that is forced with data simulated by the Urban Weather Generator.

In our case, the benefits of two-way coupling in terms of improved accuracy are negligible, because the simulated anthropogenic flux (Qf, averaging 20 W/m^2) is much smaller than the sensible heat flux (Qh, which reaches 200–300 W/m2 at noon) and the net radiant balance (Q*, which can be 600–700 W/m^2). See further details in the Supplementary Information. Although we do not have in-situ flux measurements to validate the simulated values of anthropogenic heat, it is encouraging to see that the mean annual value for the urban area obtained by this method is approximately 20 W/m^2, about the same as the figure obtained by Sailor et al. (2015) for Rome, Italy, which has similar heating and cooling requirements and a similar population density.

It is also not possible to validate the contribution of vehicles without traffic counts, which are not available for this neighborhood. However, because the magnitude of the flux – less than 10 W/m^2 at all times – is much smaller than other components of the surface energy balance, any error introduced by the lack of data is proportionately very small, too. This may be why other urban climate models, including ENVI-met, TEB and urbanized versions of WRF, do not simulate it at all.

The significance of the results is tempered by the fact that the energy requirement for HVAC in the Ramat Aviv area is quite moderate. Heating requirements are small compared to most temperate climate zone locations, and even air conditioning, which has in recent years become widespread, imposes only a modest electricity requirement. The simulation shows that both the total electricity consumption and the change due to urban effects (relative to the rural reference) are fairly small in *absolute* terms: Average heating loads for the 'standard' building are reduced by only 3.5 kWh/m^2/year, while building cooling loads increase by 2.2 kWh/m^2/year. Buildings constructed in compliance with more stringent requirements, such as 'green' buildings complying with SI 5281, are expected to consume even less electricity. However, in *relative* terms, the differences may be considered more significant: the reduction in estimated heating for the 3 building types is 47–54%, and the increase in cooling is 15–17%. Since air conditioning comprises

about 35% of electricity demand in Israel in summer, a 16% error in estimating building energy demand is equivalent to an error of nearly 6% in estimating total electricity demand. This difference is too large to ignore when assessing the potential impact of increased urban density.

It should be noted that in Israel, heating and air conditioning are both provided by reverse cycle (split) air conditioners. In both modes, the simulations assign a fixed coefficient of performance (COP) of 3.0. Lighting loads are estimated at 5 W/m^2, in the evening hours only. The output of the simulation is thus expected electricity demand, rather than the physical flows of energy through the building envelope. This reflects reality in Israel, and especially in Tel Aviv, where fuel-based heating (oil or gas) is practically non-existent. This convention is convenient for the Israeli planning authorities or homeowners using the rating tool. However, it also means that the loads reported here refer to on-site consumption and may be lower than values reported in other studies performed in cold climates where site energy consumption includes home heating based on natural gas, (diesel) fuel or even coal.

It should also be emphasized that the relative magnitude of changes in heating and cooling are purely coincidental. They are the outcome of a specific combination of inputs to the simulation, including the local climate and the construction characteristics of the building. Different inputs might result in a different balance of heating and cooling.

Current building energy standards do not specify land cover in the vicinity of the building. Plant surfaces, which will typically be cooler during daytime hours than paved surfaces, will thus emit less infrared radiation, and will thus reduce thermal loads on the adjacent buildings. This effect is not accounted for explicitly in the standard. In hot climates, HVAC loads may thus be under-estimated in dense urban locations and over-estimated in green (suburban) locations.

Urban heat island mitigation is a highly topical issue. Several strategies are often discussed in this context, such as increasing albedo and adding vegetation. To select the most suitable strategy at the neighborhood or urban scale, it is essential to assess its benefit in a given location, considering climate, building construction and other local characteristics. To this end, we have proposed a methodology that accounts for urban effects, reflected in differences between a typical reference weather station, which may be located at the airport, and a dense urban location. Such 'urbanized' weather files are not typically available to building air conditioning engineers, who rely on standard weather files such as ASHRAE's.epw files (in EnergyPlus format). Furthermore, the effect of adjacent buildings on solar exposure may not always be modelled, and such modelling is not in fact required by the building code in Israel (as well as most other countries, to the best of our knowledge). As we have shown, the magnitude of the urban effects and the effect of shading by adjacent buildings may be larger than the effect of the mitigation strategy proposed – yet these are not often considered at all. There are hundreds of studies on the effects of mitigation strategies on urban air temperature - see for example the Krayenhoff et al. [52] – yet very few of these studies combine a detailed annual simulation at an hourly resolution of the effect on building energy consumption. Jin et al. [77] is a relevant but very recent exception. As our study shows, the annual balance between heating increases and cooling savings may not justify the intervention on this basis alone (there are other very valid reasons for increasing vegetation cover).

5. Conclusions

The research presents a comprehensive methodology for establishing the effect of interventions in the urban fabric to 'mitigate' the urban heat island on building energy consumption. Any such process should necessarily account, by means of appropriate software tools, for both urban effects and building effects, and should consider conditions all year round. Urban air temperature modification due to street geometry, described by the aspect ratio H/W, shows the expected diurnal pattern with a well-developed nocturnal island and a weak daytime cool island. The urban effect on annual energy consumption depends on the balance between demand for summer cooling, which is aggravated due to the nocturnal heat, and moderated by reduced winter demand for heating. In the case of the Ramat Aviv suburb of Tel Aviv, the net effect was a small decrease in energy demand due to the urban effect, which was greatest for 'standard' buildings and lower for higher quality 'green buildings'. Increasing the green fraction to 50% yielded an average annual temperature reduction of about 0.25 °C relative to the existing condition, and a further small reduction in building energy consumption equivalent to about 2–3% of the total annual demand for heating and cooling. In contrast, a scenario with no vegetation would lead to an increase of about 0.42 °C in the mean annual air temperature, and an increase of about 1.5–1.7% in the combined demand for heating and cooling.

CRediT authorship contribution statement

Evyatar Erell: Conceptualization, Data curation, Formal analysis, Funding acquisition, Investigation, Methodology, Software, Validation, Writing – original draft, Writing – review & editing. **Bin Zhou:** Writing – review & editing, Visualization, Validation, Software, Investigation, Formal analysis, Data curation.

Declaration of competing interest

The authors declare the following financial interests/personal relationships which may be considered as potential competing interests:

Evyatar Erell reports financial support was provided by Israel Ministry of Science, Technology and Space. Evyatar Erell reports financial support was provided by Jewish National Fund. Bin Zhou reports was provided by PBC Fellowship Program for outstanding Chinese and Indian post-doctoral students. Evyatar Erell reports a relationship with University of Adelaide that includes: travel reimbursement.

Acknowledgements

This study was funded by the Israel Ministry of Science, Technology and Space, under contract # 63365 and by the Jewish National Fund through the Center for Water Sensitive Cities in Israel. Dr. Zhou was supported by the postdoctoral scholarship of the Kreitman School for Advanced Graduate Studies of the Ben-Gurion University of the Negev and the PBC Fellowship Program for outstanding Chinese and Indian post-doctoral students.

Appendix A. Supplementary data

Supplementary data to this article can be found online at https://doi.org/10.1016/j.buildenv.2022.108867.

AppendixSimulation inputs

Table A1
Configuration of CAT inputs. (For further details see Kaplan et al., 2016; Leaf and Erell, 2018; Zhou et al., 2019)

Characteristics of urban canyon site	source	value used/range					
Mean surface albedo ground	remote sensing [78]	0.11–0.53					
Mean surface albedo walls	assumption/literature	0.3					
Mean street width [m]	GIS	10–150					
Mean building height [m]	GIS	3–61					
Mean street orientation [°]	GIS	0–180					
Heat storage coefficients	[63]	Ground (A1): 0.22					
		Ground (A2): 0.33					
		Ground (A3): 20.0					
		Wall 1,2 (A1): 0.83					
		Wall 1,2 (A2): 0.40					
		Wall 1,2 (A3): 53.0					
Mixing ratio for atmos. conditions	[62,65]		rural	urban			
		Super stable	0.41	0.11			
		Inversion	0.55	0.55			
		Stable	0.76	0.75			
		Neutral	0.76	0.90			
		Turbulent	0.90	0.90			
LUMPS Beta value	[58]	5					
Plant and water fraction [%]		0–100					
Type of surface cover		loam	clay	sand	peat	pavement	mixed
Surface thermal conductivity of soil [$W \cdot m^{-1} \cdot K^{-1}$]		0.50	0.25	0.30	0.06	2.00	1.80
Volumetric heat capacity [$MJ \cdot m^{-3} \cdot K^{-1}$]		1.35	1.40	1.30	0.60	1.35	1.21
Bulk density, dry [$kg \cdot m^{-3}$]		1600	1600	1600	300	1600	1600
Infiltration coefficient		0.20	0.10	0.80	0.80	0.05	0.10
Initial soil moisture content		0.10	0.10	0.10	0.10	0.02	0.05
Maximum soil moisture content		0.40	0.40	0.40	0.8	0.05	0.2
		Dominant type of plant					
		none	grass	succulents	bushes	trees	
Stomatal resistance [$s \cdot m^{-1}$]		100	50	200	50	50	

Table A2
Building thermal properties.

element	description	U-value
'standard' building:		
walls	20 cm hollow concrete block, plastered on both sides	2.1
roof	14 cm concrete slab with light weight screed sloped to drains (avg. thickness 10 cm) and medium coloured water-proofing layer	2.6
windows	Clear single-glazed, aluminium frame. Shading: external blinds, 0.5 open in winter, 0.4 open in summer.	5.9
'green' building:		
walls	20 cm aerated concrete block, plastered on both sides	0.83
roof	14 cm concrete slab with 5 cm polystyrene insulation, light weight screed sloped to drains (avg. thickness 10 cm) and medium coloured water-proofing layer	0.69
windows	Clear double-glazed low-e, aluminium frame. SHGC: 0.52. Shading: external blinds, 0.8 open in winter, 0.4 open in summer.	3.14
'curtain wall' building:		
walls	Lightweight insulated panels with external glazing	0.66
roof	14 cm concrete slab with 5 cm polystyrene insulation, light weight screed sloped to drains (avg. thickness 10 cm) and medium coloured water-proofing layer	0.69
windows	Double-glazed solar control low-e, aluminium frame. SHGC: 0.35. No external shading.	1.8

Table A3
Internal loads for simulation of electricity consumption for HVAC and lighting in apartment buildings (all values conform to Israel Standard SI5282 – Energy Rating of Buildings).

Description	Assigned load (watts)
Human occupancy - Light activity (16:00–24:00) 125 W/person - Sleep (24:00–8:00) 80 W/person	1 occupant for each 25 m^2 of floor area, minimum of 4 and maximum of 8.
Fixed plug loads	1 W/m^2 of floor area (0.75 W/m^2 for apartments >150 m^2).
Intermittent plug loads (from 16:00–24:00)	8 W/m^2 of floor area (6 W/m^2 for apartments >150 m^2).
Mechanical comfort ventilation (from 16:00–24:00)	1 W/m^2 per fan
Mechanical night ventilation	0.06 W/m^3, multiplied by no. of ACH (which varies according to climate zone)
Lighting	5 W/m^2

Notes.
Buildings are assumed to be occupied from 16:00 until 08:00. Infiltration is estimated at a (fixed) rate of 1 ach. Air conditioning set points are 20 °C in winter and 24 °C in summer. Both heating and cooling are provided by reverse-cycle (split) air conditioning units with a rated COP of

3.0 in both heating and cooling operation. In accordance with Israel Standard 5282 (Energy Rating of Buildings), each apartment is simulated as a single thermal zone with an 'Ideal Loads Air System', which allows us to study the performance of a building without modelling a full HVAC system. The cooling sensible heat ratio, which is a simplified method for treating internal and external latent heat loads, is 0.7 (the default value in EnergyPlus).

References

[1] S. Peng, S. Piao, P. Ciais, P. Friedlingstein, C. Ottle, F.M. Bréon, H. Nan, L. Zhou, R. B. Myneni, Surface urban heat island across 419 global big cities, Environ. Sci. Technol. 46 (2012) 696–703, https://doi.org/10.1021/es2030438.

[2] T. Susca, S.R. Gaffin, G.R. Dell'Osso, Positive effects of vegetation: urban heat island and green roofs, Environ. Pollut. 159 (2011) 2119–2126, https://doi.org/10.1016/j.envpol.2011.03.007.

[3] P. Vahmani, J. Geophys. Res. Atmos. 121 (2016) 1511–1531, https://doi.org/10.1038/175238c0.

[4] A. Onishi, X. Cao, T. Ito, F. Shi, H. Imura, Evaluating the potential for urban heat-island mitigation by greening parking lots, Urban For. Urban Green. 9 (2010) 323–332, https://doi.org/10.1016/j.ufug.2010.06.002.

[5] D. Li, W. Liao, A.J. Rigden, X. Liu, D. Wang, S. Malyshev, E. Shevliakova, Urban heat island: aerodynamics or imperviousness? Sci. Adv. 5 (2019) 1–5, https://doi.org/10.1126/sciadv.aau4299.

[6] C. Wang, Z.H. Wang, J. Yang, Cooling effect of urban trees on the built environment of contiguous United States, Earth's Future 6 (2018) 1066–1081, https://doi.org/10.1029/2018EF000891.

[7] S. Oliveira, H. Andrade, T. Vaz, The cooling effect of green spaces as a contribution to the mitigation of urban heat: a case study in Lisbon, Build. Environ. 46 (2011) 2186–2194, https://doi.org/10.1016/j.buildenv.2011.04.034.

[8] W. Ouyang, T.E. Morakinyo, C. Ren, E. Ng, The cooling efficiency of variable greenery coverage ratios in different urban densities: a study in a subtropical climate, Build. Environ. (2020) 174, https://doi.org/10.1016/j.buildenv.2020.106772.

[9] M.P. Adams, P.L. Smith, A systematic approach to model the influence of the type and density of vegetation cover on urban heat using remote sensing, Landsc. Urban Plann. 132 (2014) 47–54, https://doi.org/10.1016/j.landurbplan.2014.08.008.

[10] R. Emmanuel, A. Loconsole, Landscape and urban planning green infrastructure as an adaptation approach to tackling urban overheating in the glasgow clyde valley region , UK, Landsc. Urban Plann. 138 (2015) 71–86, https://doi.org/10.1016/j.landurbplan.2015.02.012.

[11] E. Ng, L. Chen, Y. Wang, C. Yuan, A study on the cooling effects of greening in a high-density city: an experience from Hong Kong, Build. Environ. 47 (2012) 256–271, https://doi.org/10.1016/j.buildenv.2011.07.014.

[12] C. Skelhorn, S. Lindley, G. Levermore, The impact of vegetation types on air and surface temperatures in a temperate city: a fine scale assessment in Manchester, UK, Landsc. Urban Plann. 121 (2014) 129–140, https://doi.org/10.1016/j.landurbplan.2013.09.012.

[13] Z. Wang, X. Zhao, J. Yang, J. Song, Cooling and energy saving potentials of shade trees and urban lawns in a desert city, Appl. Energy 161 (2016) 437–444, https://doi.org/10.1016/j.apenergy.2015.10.047.

[14] D. Zhou, J. Xiao, S. Bonafoni, C. Berger, K. Deilami, Y. Zhou, S. Frolking, R. Yao, Z. Qiao, J.A. Sobrino, Satellite remote sensing of surface urban heat islands: progress, challenges, and perspectives, Rem. Sens. 11 (2019) 1–36, https://doi.org/10.3390/rs11010048.

[15] T.R. Oke, The energetic basis of the urban heat island, Q. J. R. Meteorol. Soc. 108 (1982) 1–24, https://doi.org/10.1002/qj.49710845502.

[16] T.R. Oke, Canyon geometry and the nocturnal urban heat island: comparison of scale model and field observations, J. Climatol. 1 (1981) 237–254, https://doi.org/10.1002/JOC.3370010304.

[17] R.A. Spronken-Smith, T.R. Oke, The thermal regime of urban parks in two cities with different summer climates, Int. J. Rem. Sens. 19 (1998) 2085–2104, https://doi.org/10.1080/014311698214884.

[18] X. Li, L.K. Norford, Urban Climate Evaluation of cool roof and vegetations in mitigating urban heat island in a tropical city , Singapore, Urban Clim. 16 (2016) 59–74, https://doi.org/10.1016/j.uclim.2015.12.002.

[19] S.H. Lee, H. Lee, S.B. Park, J.W. Woo, D. Il Lee, J.J. Baik, Impacts of in-canyon vegetation and canyon aspect ratio on the thermal environment of street canyons: numerical investigation using a coupled WRF-VUCM model, Q. J. R. Meteorol. Soc. 142 (2016) 2562–2578, https://doi.org/10.1002/qj.2847.

[20] Y. Chen, N.H. Wong, Thermal benefits of city parks, Energy Build. 38 (2006) 105–120, https://doi.org/10.1016/j.enbuild.2005.04.003.

[21] C.R. Chang, M.H. Li, S.D. Chang, A preliminary study on the local cool-island intensity of Taipei city parks, Landsc. Urban Plann. 80 (2007) 386–395, https://doi.org/10.1016/j.landurbplan.2006.09.005.

[22] X. Cao, A. Onishi, J. Chen, H. Imura, Quantifying the cool island intensity of urban parks using ASTER and IKONOS data, Landsc. Urban Plann. 96 (2010) 224–231, https://doi.org/10.1016/j.landurbplan.2010.03.008.

[23] D.E. Bowler, L. Buyung-Ali, T.M. Knight, A.S. Pullin, Urban greening to cool towns and cities: a systematic review of the empirical evidence, Landsc. Urban Plann. 97 (2010) 147–155, https://doi.org/10.1016/j.landurbplan.2010.05.006.

[24] M. Bruse, H. Fleer, Simulating surface-plant-air interactions inside urban environments with a three dimensional numerical model, Environ. Model. Software 13 (1998) 373–384, https://doi.org/10.1016/S1364-8152(98)00042-5.

[25] S. Thorsson, F. Lindberg, Different Methods for Estimating the Mean Radiant Temperature in an Outdoor Urban Setting, 2007, pp. 1983–1993, https://doi.org/10.1002/joc, 1993.

[26] P. Höppe, The physiological equivalent temperature - a universal index for the biometeorological assessment of the thermal environment, Int. J. Biometeorol. 43 (1999) 71–75, https://doi.org/10.1007/s004840050118.

[27] A. Matzarakis, H. Mayer, M.G. Iziomon, Applications of a universal thermal index: physiological equivalent temperature, Int. J. Biometeorol. 43 (1999) 76–84, https://doi.org/10.1007/s004840050119.

[28] P. Bröde, D. Fiala, K. Błażejczyk, I. Holmér, G. Jendritzky, B. Kampmann, B. Tinz, G. Havenith, Deriving the operational procedure for the universal thermal climate index (UTCI), Int. J. Biometeorol. 56 (2012) 481–494, https://doi.org/10.1007/s00484-011-0454-1.

[29] R. Emmanuel, A. Loconsole, Green infrastructure as an adaptation approach to tackling urban overheating in the Glasgow Clyde Valley Region, UK, Landsc. Urban Plann. 138 (2015) 71–86, https://doi.org/10.1016/j.landurbplan.2015.02.012.

[30] A. Middel, K. Häb, A.J. Brazel, C.A. Martin, S. Guhathakurta, Impact of urban form and design on mid-afternoon microclimate in Phoenix Local Climate Zones, Landsc. Urban Plann. 122 (2014) 16–28, https://doi.org/10.1016/j.landurbplan.2013.11.004.

[31] E. Ng, L. Chen, Y. Wang, C. Yuan, A study on the cooling effects of greening in a high-density city: an experience from Hong Kong, Build. Environ. 47 (2012) 256–271, https://doi.org/10.1016/j.buildenv.2011.07.014.

[32] K. Perini, A. Magliocco, Effects of vegetation, urban density, building height, and atmospheric conditions on local temperatures and thermal comfort, Urban For. Urban Green. 13 (2014) 495–506, https://doi.org/10.1016/j.ufug.2014.03.003.

[33] M. Taleghani, D. Sailor, G.A. Ban-Weiss, Micrometeorological simulations to predict the impacts of heat mitigation strategies on pedestrian thermal comfort in a Los Angeles neighborhood, Environ. Res. Lett. 11 (2016) 24003, https://doi.org/10.1088/1748-9326/11/2/024003.

[34] D.B. Crawley, J.W. Hand, M. Kummert, B.T. Griffith, Contrasting the capabilities of building energy performance simulation programs, Build. Environ. 43 (2008) 661–673, https://doi.org/10.1016/j.buildenv.2006.10.027.

[35] S. Wilcox, W. Marion, Users Manual for TMY3 Data Sets, 2008.

[36] E. Erell, T. Williamson, Simulating air temperature in an urban street canyon in all weather conditions using measured data at a reference meteorological station, Int. J. Climatol. 26 (2006) 1671–1694, https://doi.org/10.1002/JOC.1328.

[37] B. Bueno, L. Norford, J. Hidalgo, G. Pigeon, The urban weather generator, J. Build. Perform. Simulat. 6 (2013) 269–281, https://doi.org/10.1080/19401493.2012.718797.

[38] D.B. Crawley, Estimating the impacts of climate change and urbanization on building performance, J. Build. Perform. Simulat. 1 (2008) 91–115, https://doi.org/10.1080/19401490802182079.

[39] H. Saaroni, E. Ben-dor, A. Bitan, O. Potchter, Spatial distribution and microscale characteristics of the urban heat island in Tel-Aviv, Israel 48 (2000) 1–18.

[40] E. Erell, T. Williamson, Intra-urban differences in canopy layer air temperature at a mid-latitude city, Int. J. Climatol. 27 (2007) 1243–1255, https://doi.org/10.1002/joc.1469.

[41] A.M. Coutts, J. Beringer, N.J. Tapper, Impact of increasing urban density on local climate: spatial and temporal variations in the surface energy balance in Melbourne, Australia, J. Appl. Meteorol. Climatol. 46 (2007) 477–493, https://doi.org/10.1175/JAM2462.1.

[42] I.D. Stewart, T.R. Oke, Local climate zones for urban temperature studies, Bull. Am. Meteorol. Soc. 93 (2012) 1879–1900, https://doi.org/10.1175/BAMS-D-11-00019.1.

[43] D.J. Sailor, N. Dietsch, The urban heat island mitigation impact screening tool (MIST), Environ. Model. Software 22 (2007) 1529–1541, https://doi.org/10.1016/j.envsoft.2006.11.005.

[44] A. Coutts, J. Beringer, N.J. Tapper, Investigating the climatic impact of urban planning strategies through the use of regional climate modelling: a case study for Melbourne, Australia, Int. J. Climatol. 28 (2008) 1943–1957.

[45] E. Erell, The application of urban climate research in the design of cities, Adv. Build. Energy Res. 2 (2008), https://doi.org/10.3763/aber.2008.0204.

[46] E. Erell, D. Pearlmutter, T. Williamson, Urban Microclimate: Designing the Spaces between Buildings, Earthscan, London, 2011.

[47] N. Lauzet, A. Rodler, M. Musy, M.H. Azam, S. Guernouti, D. Mauree, T. Colinart, How building energy models take the local climate into account in an urban

context – a review, Renew. Sustain. Energy Rev. 116 (2019) 109390, https://doi.org/10.1016/J.RSER.2019.109390.
[48] G. Mills, H. Cleugh, R. Emmanuel, W. Endlicher, E. Erell, G. McGranahan, E. Ng, A. Nickson, J. Rosenthal, K. Steemer, Climate information for improved planning and management of mega cities (Needs Perspective), in: Procedia Environmental Sciences, 2010, https://doi.org/10.1016/j.proenv.2010.09.015.
[49] E. Erell, Urban greening and microclimate modification, in: T.P. Yok, C.Y. Jim (Eds.), Greening Cities – Forms and Functions, Springer Nature, Singapore, 2017.
[50] E.G. Mcpherson, Impact Veg. Resid. Heat. Cool. 12 (1988) 41–51.
[51] L. Shashua-Bar, D. Pearlmutter, E. Erell, The cooling efficiency of urban landscape strategies in a hot dry climate, Landsc. Urban Plann. 92 (2009) 179–186, https://doi.org/10.1016/j.landurbplan.2009.04.005.
[52] E.S. Krayenhoff, A.M. Broadbent, L. Zhao, M. Georgescu, A. Middel, J.A. Voogt, A. Martilli, D.J. Sailor, E. Erell, Cooling hot cities: a systematic and critical review of the numerical modelling literature, Environ. Res. Lett. 16 (2021), 053007, https://doi.org/10.1088/1748-9326/ABDCF1.
[53] J. Yang, E. Bou-Zeid, Scale dependence of the benefits and efficiency of green and cool roofs, Landsc. Urban Plann. 185 (2019) 127–140, https://doi.org/10.1016/J.LANDURBPLAN.2019.02.004.
[54] F. Salamanca, A. Krpo, A. Martilli, A. Clappier, A new building energy model coupled with an urban canopy parameterization for urban climate simulations-part I. formulation, verification, and sensitivity analysis of the model, Theor. Appl. Climatol. 99 (2010) 331–344, https://doi.org/10.1007/s00704-009-0142-9.
[55] F. Salamanca, A. Martilli, A new Building Energy Model coupled with an Urban Canopy Parameterization for urban climate simulations-part II. Validation with one dimension off-line simulations, Theor. Appl. Climatol. 99 (2010) 345–356, https://doi.org/10.1007/S00704-009-0143-8/TABLES/8.
[56] F. Chen, H. Kusaka, R. Bornstein, J. Ching, C.S.B. Grimmond, S. Grossman-Clarke, T. Loridan, K.W. Manning, A. Martilli, S. Miao, D. Sailor, F.P. Salamanca, H. Taha, M. Tewari, X. Wang, A.A. Wyszogrodzki, C. Zhang, The integrated WRF/urban modelling system: development, evaluation, and applications to urban environmental problems, Int. J. Climatol. 31 (2011) 273–288, https://doi.org/10.1002/joc.2158.
[57] D. Mauree, N. Blond, A. Clappier, Multi-scale modeling of the urban meteorology: integration of a new canopy model in the WRF model, Urban Clim. 26 (2018) 60–75, https://doi.org/10.1016/J.UCLIM.2018.08.002.
[58] E. Erell, T. Williamson, Simulating air temperature in an urban street canyon in all weather conditions using measured data at a reference meteorological station, Int. J. Climatol. 26 (2006) 1671–1694, https://doi.org/10.1002/joc.1328.
[59] S. Kaplan, A. Peeters, E. Erell, Predicting air temperature simultaneously for multiple locations in an urban environment: a bottom up approach, Appl. Geogr. 76 (2016) 62–74, https://doi.org/10.1016/j.apgeog.2016.09.015.
[60] B. Zhou, S. Kaplan, A. Peeters, I. Kloog, E. Erell, "Surface," "satellite" or "simulation": mapping intra-urban microclimate variability in a desert city, Int. J. Climatol. (2019), https://doi.org/10.1002/joc.6385.
[61] A. Yezioro, O. Shapir, G. Capeluto, A simple user interface for energy rating of buildings, Proc. Build. Simulat. 2011 (2011) 1293–1298.
[62] E. Erell, I. Eliasson, S. Grimmond, B. Offerle, T. Williamson, The effect of stability on estimated variations of advcted moisture in the canyon air temperature (CAT) model, in: The 9th AMS Symposium on the Urban Environment, 2010, pp. 3–8.
[63] C.S.B. Grimmond, T.R. Oke, Turbulent heat fluxes in urban areas: observations and a local-scale urban meteorological parameterization scheme (LUMPS), J. Appl. Meteorol. 41 (2002) 792–810, https://doi.org/10.1175/1520-0450(2002)041<0792:THFIUA>2.0.CO;2.
[64] J. Leaf, E. Erell, A model of the ground surface temperature for micrometeorological analysis, Theor. Appl. Climatol. 133 (2018) 697–710, https://doi.org/10.1007/s00704-017-2207-5.
[65] E. Erell, I. Eliasson, S. Grimmond, B. Offerle, T. Williamson, Incorporating spatial and temporal variations of advected moisture in the canyon air temperature (cat) model, in: The Seventh International Conference on Urban Climate, 2009, pp. 29–32.
[66] S. Liang, Narrowband to broadband conversions of land surface albedo I Algorithms, Remote Sens. Environ. 76 (2001) 213–238, https://doi.org/10.1016/S0034-4257(00)00205-4.
[67] S. Liang, C.J. Shuey, A.L. Russ, H. Fang, M. Chen, C.L. Walthall, C.S.T. Daughtry, R. Hunt, Narrowband to broadband conversions of land surface albedo: II. Validation, Remote Sens. Environ. 84 (2002) 25–41, https://doi.org/10.1016/S0034-4257(02)00068-8.
[68] L. Breiman, J.H. Friedman, R.A. Olshen, C.J. Stone, Classification and Regression Trees, Routledge, 1984, https://doi.org/10.1201/9781315139470.
[69] R.R. Core Team, R: A Language, Environment for Statistical Computing, Vienna, Austria, 2014.
[70] Esri, ArcGIS Desktop: Release 10.6 (2018).
[71] B. Zhou, S. Kaplan, A. Peeters, I. Kloog, E. Erell, "Surface," "satellite" or "simulation": mapping intra-urban microclimate variability in a desert city, Int. J. Climatol. (2019), https://doi.org/10.1002/joc.6385.
[72] D.J. Sailor, L. Lu, A top-down methodology for developing diurnal and seasonal anthropogenic heating profiles for urban areas, Atmos. Environ. 38 (2004) 2737–2748, https://doi.org/10.1016/j.atmosenv.2004.01.034.
[73] T.J. Williamson, A confirmation technique for thermal performance simulation models Building performance, Build. Simulat. (1995) 268–275.
[74] N. Artmann, H. Manz, P. Heiselberg, Climatic potential for passive cooling of buildings by night-time ventilation in Europe, Appl. Energy 84 (2007) 187–201, https://doi.org/10.1016/j.apenergy.2006.05.004.
[75] A. Yezioro, O. Shapir, G. Capeluto, A simple user interface for energy rating of buildings, Proc. Build. Simulat. 2011 (2011) 1293–1298.
[76] B. Bueno, L. Norford, G. Pigeon, R. Britter, Combining a detailed building energy model with a physically-based urban canopy model, Boundary-Layer Meteorol. 140 (3) (2011) 471–489, https://doi.org/10.1007/S10546-011-9620-6, 2011 140.
[77] L. Jin, S. Schubert, D. Fenner, F. Meier, C. Schneider, Integration of a building energy model in an urban climate model and its application, Boundary-Layer Meteorol. 178 (2) (2020) 249–281, https://doi.org/10.1007/S10546-020-00569-Y, 2020 178.
[78] S. Liang, Narrowband to broadband conversions of land surface albedo I Algorithms, Remote Sens. Environ. 76 (2001) 213–238, https://doi.org/10.1016/S0034-4257(00)00205-4.